

Cross-feeding interactions between *Fusobacterium nucleatum* and the glycan forager *Segatella oris*

Joshua R. Fletcher,¹ Areej Malik,¹ Jacob Driggers,¹ Ryan C. Hunter²

AUTHOR AFFILIATIONS See affiliation list on p. 13.

ABSTRACT *Fusobacterium nucleatum* is a common member of the oral microbiota frequently associated with extra-oral infections and diverse polymicrobial environments, including chronic airway diseases and colorectal tumors. Yet, its interactions with co-colonizing microbiota remain poorly defined. Here, we investigate cross-feeding interspecies dynamics between *F. nucleatum* and *Segatella oris*, a glycan-foraging anaerobe enriched in the airways, oral cavity, and gastrointestinal tumors. Using broth cultures, cell-free supernatants, and co-culture on primary human airway epithelial cells, we identify microbe-microbe and microbe-host interactions that shape nutrient acquisition, biofilm formation, gene expression, and host responses. While mucin or *S. oris* supernatants modestly enhanced *F. nucleatum* growth, both conditions triggered transcriptional remodeling, including induction of the *nan* operon for sialic acid catabolism, suggesting reliance on glycan degradation by *S. oris*. Conversely, *S. oris* exhibited differential expression of multiple polysaccharide utilization loci (PULs) when exposed to *F. nucleatum* or its metabolites. Biofilm formation by *F. nucleatum* was strongly inhibited by *S. oris* and its supernatants, indicative of metabolic regulation. Dual and triple RNA-seq revealed that epithelial responses were predominately shaped by *F. nucleatum*, with enrichment of inflammatory and cancer-associated pathways; however, co-colonization with *S. oris* modulated the expression of genes linked to the unfolded protein response and apoptosis, among others. These findings demonstrate that glycan-mediated cross-feeding and microbial interactions shape the physiology and pathogenic potential of *F. nucleatum* in mucosal environments. This work underscores the importance of modeling polymicrobial communities under host-relevant conditions to better understand pathobiont behavior at the epithelial interface.

IMPORTANCE *Fusobacterium nucleatum* is increasingly recognized as a pathobiont in mucosal diseases, including colorectal cancers and chronic airway infections, yet its functional interactions with co-colonizing microbiota remain poorly understood. Here, we demonstrate that *F. nucleatum* engages in bidirectional interactions with *Segatella oris*, a glycan-foraging anaerobe also enriched in mucin-rich environments. Through nutrient cross-feeding and transcriptional modulation, these interactions shape bacterial behavior and the host epithelial response. Notably, glycan degradation by *S. oris* enables *F. nucleatum* access to sialic acids, while *F. nucleatum* suppresses the expression of multiple polysaccharide utilization loci in *S. oris*, revealing a reciprocal ecological influence. Co-colonization of the airway epithelial surface also modulates gene expression linked to inflammation and cancer. These findings advance our understanding of polymicrobial dynamics at mucosal interfaces and highlight the importance of incorporating microbe-microbe-host interactions into reductionist models of infection and disease.

KEYWORDS *Fusobacterium nucleatum*, *Segatella oris*, *Prevotella oris*, cross-feeding, glycans, microbiome, chronic airway disease, transcriptomics

Editor Sarah M. Allard, University of California San Diego, La Jolla, California, USA

Address correspondence to Joshua R. Fletcher, jrfletc2@ncsu.edu.

Areej Malik and Jacob Driggers contributed equally to this article. Order was determined by authors' efforts to this work.

The authors declare no conflict of interest.

See the funding table on p. 13.

Received 20 June 2025

Accepted 5 December 2025

Published 21 January 2026

Copyright © 2026 Fletcher et al. This is an open-access article distributed under the terms of the [Creative Commons Attribution 4.0 International license](https://creativecommons.org/licenses/by/4.0/).

Fusobacterium nucleatum is a Gram-negative member of the oral microbiota that contributes to biofilm assembly, architecture, and community organization (1, 2). Although best known for its roles in dental plaque and periodontal disease, *F. nucleatum* is implicated in a range of extraoral infections and is frequently detected in tumors across multiple cancer types (3–6). While it can function as both a commensal and pathogen, *F. nucleatum* is often found in diverse polymicrobial host environments, including colorectal tumors and the airways of individuals with chronic rhinosinusitis (CRS), cystic fibrosis (CF), or chronic obstructive pulmonary disease (COPD) (7–14). This tendency raises questions about whether and how *F. nucleatum* interacts with co-colonizing microbiota and how these interactions shape its behavior and pathogenic potential. Equally important is understanding how *F. nucleatum* influences the activity of other taxa in these communities, many of which also exhibit context-dependent commensal or pathogenic behavior (15).

Segatella oris (formerly *Prevotella oris*) is also a member of the oral microbiota though less is known about its physiology or microbial interactions. Notably, *S. oris* supernatants inhibit the growth of the airway pathogen *Moraxella catarrhalis* *in vitro*, suggesting a connection between *S. oris* residence in the upper airways and colonization resistance against some pathogens (16). However, *S. oris* also exhibits pathogenic traits, including hemolysin production with activity against human erythrocytes (17). Like *F. nucleatum*, it is detected in extraoral infections, gastric tumors, CRS and CF airway mucus and is co-enriched with *F. nucleatum* in the oral microbiomes of cancer patients with chemotherapy-induced oral mucositis (9, 18, 19). More broadly, both *Fusobacterium* and *Prevotella* genera are co-detected in esophageal tumors (20), suggesting that cross-feeding interactions between these taxa may facilitate colonization and promote disease.

Although environmental conditions vary across infection sites, shared features such as host glycans, proteoglycans, and glycosaminoglycans are common. These features are particularly prevalent in mucus-laden airways of patients with chronic respiratory diseases and the mucus layer lining the intestinal tract, where *F. nucleatum* is frequently detected (21). *F. nucleatum* primarily ferments amino acids to generate ATP although glucose and fructose metabolism have also been reported (22–26). While it produces intracellular polyglucose granules *in vitro*, the genetic basis and functional significance of this pathway, including possible links to virulence, remain unclear (27). Notably, *F. nucleatum* lacks sialidases and polysaccharide utilization loci (PULs) but can scavenge sialic acids liberated by glycan foraging microbes (28), potentially enhancing community persistence through cross-feeding. In contrast, the genome of the *S. oris* type strain NCTC 13071 encodes 27 predicted PULs, likely involved in sensing, importing, and degrading of complex polysaccharides such as mucins and other host glycans (29, 30).

Given their frequent co-occurrence in mucin-rich environments *in vivo* and the possible complementarity of their metabolic repertoires, we hypothesized that *F. nucleatum* and *S. oris* engage in cross-feeding interactions. To test this, we examined how each species adjusts its growth and gene expression to mucin glycoproteins and each other's metabolic byproducts. We found that while neither mucins nor *S. oris* supernatant substantially altered the growth of *F. nucleatum*, both conditions triggered significant transcriptional changes. Conversely, *S. oris* exhibited distinct growth dynamics and widespread transcriptional responses in mucin and *F. nucleatum* supernatants. Although *F. nucleatum* forms robust biofilms, biofilm formation was greatly reduced in *S. oris* supernatants and in co-culture despite biofilm growth in mucin or control media. We further extended these analyses using co-culture of each species, individually and together, on the apical surface of primary human airway epithelial cells to model aspiration-based colonization relevant to CF, CRS, and COPD. Dual (host-*S. oris*, host-*F. nucleatum*) and triple (host-*S. oris*-*F. nucleatum*) RNA sequencing revealed that host-associated growth conditions strongly influence bacterial gene expression, including unexpected variability in *S. oris* PUL expression mediated by *F. nucleatum*. Host transcriptional responses were primarily driven by *F. nucleatum*, with prominent induction of pro-inflammatory mediators *TNFA* and *TNFAIP2*, as well as several genes linked to cancer.

Together, these data capture key information about bacterial interactions on relevant host cell types and highlight how co-colonizing, cross-feeding partners may modify each other's physiology and influence host responses.

MATERIALS AND METHODS

Bacterial strains and media conditions

Fusobacterium nucleatum subsp. *nucleatum* strain ATCC 25586 and *Segatella oris* strain NCTC13071 were propagated anaerobically in a Coy anaerobic chamber (90% nitrogen, 5% carbon dioxide, 5% hydrogen) using BBL *Brucella* broth (BD) or 1.5% agar plates supplemented with hemin (250 µg/mL) and vitamin K (50 µg/mL) (Hardy Diagnostics). A semi-defined control medium was prepared by combining *Brucella* broth with minimal salts (50:50) as previously described (31). A minimal mucin medium (MMM) was generated by autoclaving porcine gastric mucin (PGM; Sigma) at 30 g/L in water, diluting to 15 g/L in 2× minimal salts, and combining 1:1 with *Brucella* broth to yield the final mucin-containing experimental medium (hereafter referred to as mucin medium), adapted from Flynn et al. (32) with dialysis steps omitted. Cell-free supernatants (CFS) were prepared in biological triplicate by culturing each strain for 48 h in mucin medium (10 mL) under anaerobic conditions. Cultures were centrifuged at 4,000 rpm at 4°C for 20 min, and the resulting supernatants were then passed through 0.22 µm filters. CFS were stored at -80°C and thawed once immediately prior to use.

Growth curves

F. nucleatum and *S. oris* were grown overnight in *Brucella* broth supplemented with hemin (0.35 mg/mL) and vitamin K (0.05 mg/mL) and then subcultured 1:5 in fresh medium and grown for an additional 4 h. Optical density at 600 nm (OD600) was determined via spectrophotometry and adjusted to 0.01 in the respective growth medium (control, mucin, or cell-free mucin medium supernatants). Two hundred microliters of each culture was added to individual wells in a clear, flat-bottomed 96-well plate in technical triplicate across three biological replicates. Plates were sealed with a Breathe-Easy gas-permeable membrane and incubated in a Tecan Sunrise plate reader in the anaerobic chamber at 37°C for 72 h. OD600 was recorded hourly following 5 s of linear shaking. Viable bacteria were enumerated from 2 mL cultures at 0, 4, 8, and 24 h after inoculation by serial 10-fold dilution and plating onto *Brucella* agar supplemented with hemin and vitamin K. Plates were incubated anaerobically for 48 h prior to colony counting.

Biofilm assays

Biofilm assays were performed in parallel using identical media conditions as described for growth curves, following the protocol of Merritt et al. (33). Briefly, microtiter plates were inoculated with each species individually or in co-culture and incubated anaerobically at 37°C for 48 h. Following incubation, plates were removed from the chamber and planktonic cultures were discarded. Plates were washed three times with 250 µL water, stained with 200 µL 0.1% crystal violet (in water) for 15 min, and then washed again three times and air-dried overnight. Crystal violet was solubilized with 200 µL of 30% acetic acid, and absorbance at 550 nm was determined using a BioTek Synergy H1 microplate reader. Wells containing sterile media were used as negative controls for background subtraction.

Colonization of primary human airway epithelial monolayers

Normal human bronchial epithelial (NHBE) cells (Lonza Bioscience) obtained from healthy donors were expanded B-ALI Growth Basal Medium (Lonza) and seeded on 6.5 mm Transwell inserts (0.4 µm pore; STEMCELL Technologies). These cells produce mucus

in vitro, primarily MUC5AC and MUC5B, making them excellent models for bacterial glycan foraging and cross-feeding (34, 35). Upon reaching confluency after ~2–4 days post-seeding, apical medium was removed, and basolateral medium was replaced with B-ALI Differentiation Basal Medium (Lonza). Cells were maintained at air-liquid interface (ALI) for 3–4 weeks at 37°C and 5% CO₂ in a humidified incubator.

Overnight bacterial cultures were grown in *Brucella* broth supplemented with hemin and vitamin K. These were subcultured 1:5 in fresh medium and grown to OD₆₀₀ = 0.5. Cultures were diluted 1:10 into infection medium (DMEM supplemented with 2% FBS, 10 mM HEPES, 0.1 mM nonessential amino acids, 4 mM L-glutamate, and 1 mM sodium pyruvate). One hundred microliters of bacterial suspension was applied to the apical surface of each Transwell and incubated for 4 h at 37°C under anaerobic conditions, resulting in an approximate MOI of 10:1 bacteria per host cell. After incubation, apical supernatants were gently removed by pipette, and co-cultures were maintained for an additional 20h prior to RNA extraction.

RNA extraction

Each species was grown in 10 mL of control, mucin, and CFS media in 15 mL conical Falcon tubes for 24 h and collected by centrifugation at 4,000 rpm for 20 min at 4°C. Pellets were dissolved by gentle pipetting in 1 mL of TRIzol Reagent (ThermoFisher). For airway epithelial co-cultures, 250 µL TRIzol was added to the apical surface and a 1 mL pipette tip was used to scrape cellular material from the transwell surface. Scraping was performed four times per insert to yield 1 mL of total lysate in TRIzol. All TRIzol samples were incubated for 5 min at room temperature, followed by the addition of 200 µL chloroform, hand agitation for 15 s, followed by another 5-min incubation on the benchtop. Phase separation was performed by centrifugation at 12,000 rpm for 15 min at 4°C. The aqueous phase was mixed 1:1 with 95% ethanol, and RNA was column purified with the Zymo Clean & Concentrator-5 kit including an on-column DNase-I treatment according to manufacturer's instructions.

RNA sequencing and analysis

Total RNA from broth cultures was submitted to Seq Center (Pittsburgh, PA), where rRNA depletion was performed with the Illumina Stranded Total RNA Prep with Ribo-Zero Plus Microbiome kit prior to library preparation and sequencing (2 × 150 bp). RNA from bacterial and epithelial co-cultures was sent to SeqCoast Genomics (Portsmouth, NH). rRNA depletion was also performed on these samples prior to Illumina sequencing (2 × 150 bp). Sequencing was performed on the Illumina NextSeq2000 platform with a 300 cycle flow cell kit. Read quality was assessed using FastQC (<https://www.bioinformatics.babraham.ac.uk/projects/fastqc/>). Given the consistently high quality and the risk of biasing downstream analyses (36), no read trimming was performed.

For bacterial RNA seq, coding sequences for all annotated genes and riboswitches, gene names, and locus tags were extracted from the *F. nucleatum* ATCC 25586 (NZ_CP028101) and *S. oris* NCTC 17031 (NZ_LR134384) genomes in Geneious Prime (2024.0.7) and converted to FASTA format via the "Tabular-to-fasta" tool via the Galaxy server (<https://usegalaxy.org/>), and indexed with Salmon (37) for quasi-mapping of reads. For host RNA-seq, the *Homo sapiens* transcriptome (GRCh38.p14, release 45) was retrieved from Gencode (https://www.gencodegenes.org/human/release_45.html). Transcriptome indices were built in Salmon, to which reads were quasi-mapped. The quant.sf files generated by Salmon were imported into RStudio via the tximport package (38), and differential expression analysis was performed with DESeq2 (39). The threshold for differential expression was a log₂ fold change ≥1 at an adjusted *P*-value <0.05. Code for each analysis is available at https://github.com/Hunter-Lab-UMN/Fletcher_FnSo_2025.

RESULTS

Growth and biofilm formation of *F. nucleatum* and *S. oris* are influenced by mucin and cross-feeding *in vitro*

F. nucleatum and *S. oris* were cultured under three conditions: (i) control medium, (ii) control medium supplemented with porcine gastric mucin (hereafter “mucin medium”), or (iii) cell-free supernatants (CFS) derived from each species grown in mucin medium for 48 h. In the control medium, *F. nucleatum* exhibited distinct growth phases with a pronounced exponential phase followed by stationary and death phases, with optical density remaining consistent after ~36 h. Exponential growth rates were similar across conditions; however, cultures grown in mucin medium or *S. oris* CFS reached higher stationary-phase densities and exhibited a slower decline during death phase compared to controls (~12–36 h; Fig. 1A). This elevated density in mucin medium was sustained until ~60 h, after which it declined to control levels. Area-under-curve (AUC) analysis reflected this trend, with mucin medium showing a modest, though not statistically significant, increase relative to the control ($P = 0.0951$; Fig. 1B). In contrast, *F. nucleatum* density in *S. oris* CFS declined sharply after 48 h, yielding an AUC comparable to the control. Experiments were repeated in larger culture volumes, and CFUs were enumerated at 0, 4, 8, and 24 h (Fig. S1A and B). Each strain grew well in all media, with *S. oris* CFUs being more consistent between conditions than was apparent during growth in microtiter plates.

Biofilm formation by *F. nucleatum* was robust in both control and mucin media, with a trend toward increased biofilm in mucin medium. However, biofilm growth was nearly abolished in *S. oris* CFS (Fig. 1C). Although nutrient depletion in *S. oris* CFS could partially contribute to reduced biofilm formation, this is unlikely given that *F. nucleatum* exhibited comparable planktonic growth in CFS and control medium. These findings suggest that *S. oris* produces one or more metabolites that inhibit *F. nucleatum* biofilm development. This suppression is unexpected given *F. nucleatum*'s well-established role as a so called bridging species in the highly structured and spatially stratified polymicrobial biofilms of the oral cavity (40).

In contrast, *S. oris* exhibited markedly different growth dynamics across conditions. Growth in control medium was slow with apparent diauxie following a brief stationary phase at ~24 h, a second exponential phase, and final plateau at ~40 h (Fig. 1D). This pattern may reflect initial depletion of readily metabolizable sugars followed by utilization of more complex structures such as mucin glycans, consistent with its predicted PUL repertoire. In mucin medium, *S. oris* grew much more rapidly, reaching a higher maximum density and exhibiting a threefold increase in AUC compared to the control (Fig. 1E). Likewise, diminished growth in *F. nucleatum* CFS could result from reduced availability of simple carbohydrates though the enhanced growth in mucin medium suggests that *S. oris* efficiently forages host glycans when preferred carbon sources are limited. These findings are consistent with genomic predictions of glycan utilization via PULs. Growth in *F. nucleatum* CFS yielded a faster growth rate than control medium but lower stationary phase density than mucin medium; AUC for CFS and control were comparable. Biofilm formation by *S. oris* was minimal in the control medium and nearly undetectable in mucin medium or CFS conditions (Fig. 1F). In dual-species cultures grown in control or mucin media, biofilms phenocopied the minimal single-species biofilms of *S. oris* (Fig. S1).

F. nucleatum and *S. oris* transcriptomes are modulated by mucin medium, cross-feeding, and interactions with human airway epithelia

Both species exhibited growth phenotypes responsive to the nutritional composition of each medium (Fig. 1). Mucin supplementation modestly enhanced *F. nucleatum* growth but had a pronounced effect on *S. oris*, suggesting species-specific nutrient utilization. Growth in CFS derived from either species grown in mucin medium was comparable to or greater than growth in the control medium, indicating that neither species fully

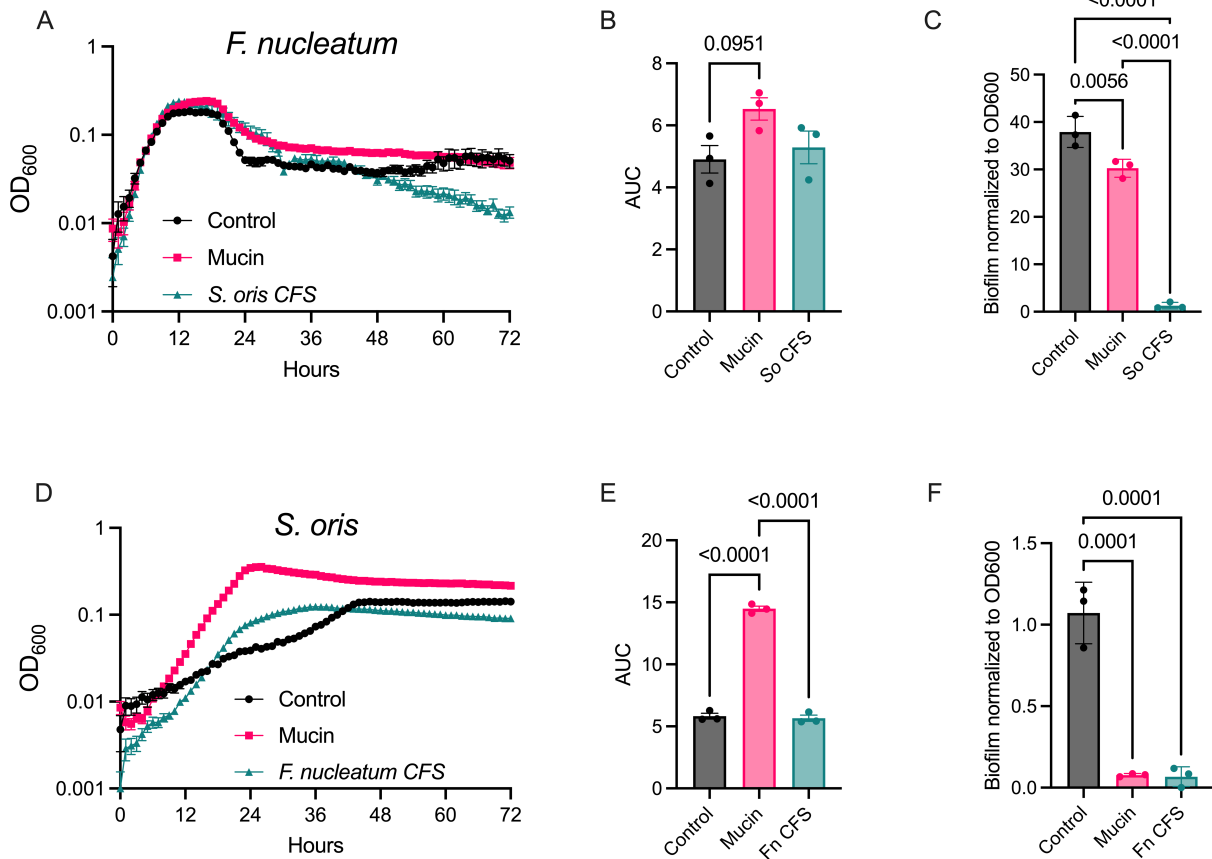


FIG 1 Mucin and interspecies metabolite exchange influence growth and biofilm formation of *F. nucleatum* and *S. oris*. (A) Growth curves of *F. nucleatum* in control medium, mucin medium, and *S. oris* cell-free supernatants (CFS) ($n = 3$). (B) Area under the curve (AUC) analysis for *F. nucleatum* growth. (C) Biofilm formation by *F. nucleatum* in each condition after 48 h, quantified by crystal violet staining. (D) Growth curves of *S. oris* in control medium, mucin medium, and *F. nucleatum* CFS. (E) AUC analysis for *S. oris* growth. (F) Biofilm formation by *S. oris* across all conditions. Data represent the mean of three biological replicates \pm standard error of the mean ($n = 3$). Statistical significance in panels B, C, E, and F was determined using ordinary one-way ANOVA with Tukey's multiple comparisons test. Error bars in panels A and D are the standard error of the mean (SEM).

exhausted nutrients essential to the other. Interestingly, *S. oris* growth was diminished in *F. nucleatum* CFS compared to mucin medium despite *F. nucleatum* lacking known glycan-degrading capabilities. Given their potential clinical relevance and prevalence of each species in chronic airway disease, we also sought to connect broth culture data to more physiologically relevant conditions with host airway epithelia. To model how each species influences the host airway response to colonization, we employed our recently described Dual Oxidic-Anoxic Co-Culture (DOAC) model, in which oxygen-dependent airway epithelial cells are supplied oxygenated blood gas basolaterally while exposing their apical surfaces to the anaerobic chamber environment (41). This advancement allows for colonization and growth of obligate anaerobes on epithelial cells, enabling study of host-pathogen-microbiota interactions. We performed RNA-seq on each bacterium in control, mucin, and CFS media, as well as dual- and triple RNA-seq on primary normal human bronchial epithelial (NHBE) cells challenged with each bacterium alone or in co-culture for 24 h. This allowed us to determine how different growth environments affect the expression of genes involved in nutrient acquisition and metabolism. Differentially expressed genes are provided in File S1 (*F. nucleatum*) and File S2 (*S. oris*) and visualized in MA plots in Fig. S2 and S6. Principal component analysis (Fig. 2A and 3A) revealed that the greatest transcriptomic separation occurred between broth cultures media and airway epithelial co-cultures, with CFS exerting the most pronounced transcriptional shift among media conditions.

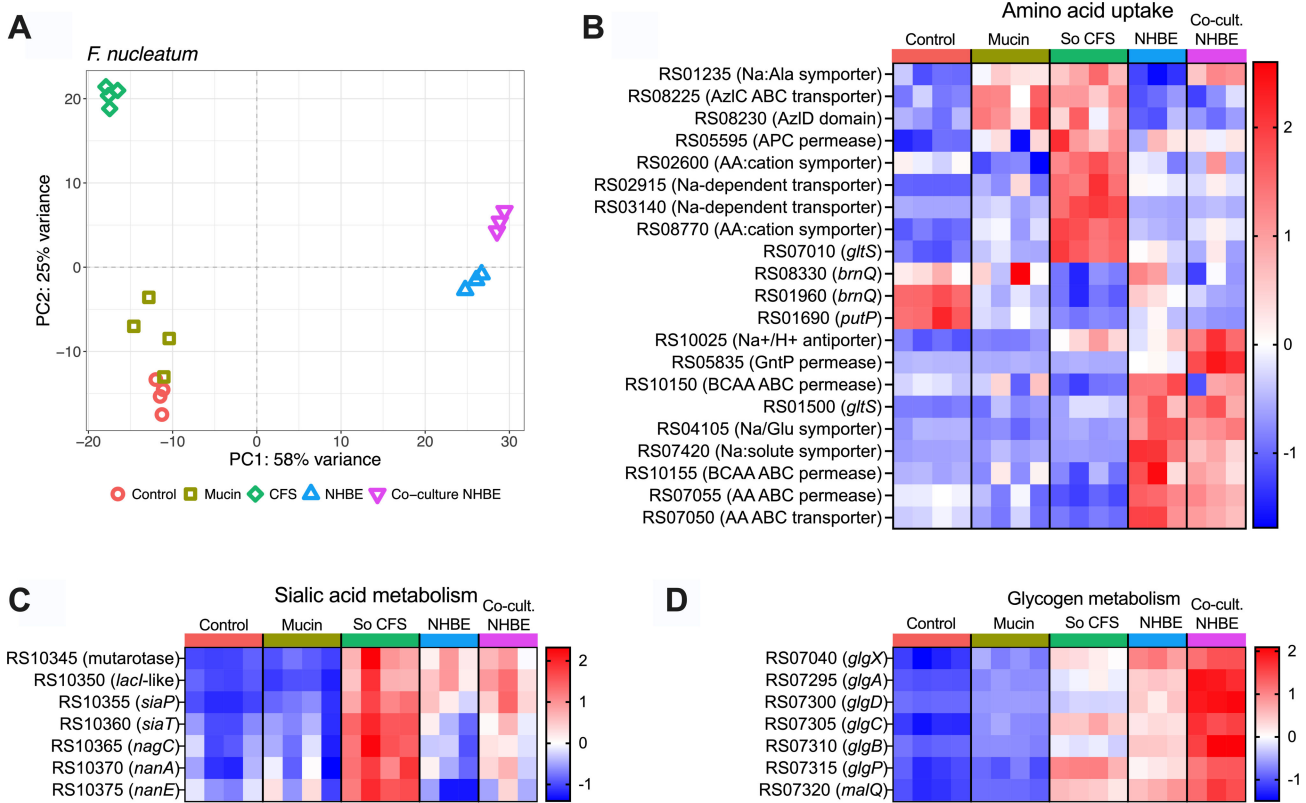


FIG 2 Transcriptomic responses of *F. nucleatum* to mucin, *S. oris* supernatants, and epithelial co-culture is (A) Principal component analysis (PCA) of *F. nucleatum* transcriptomes across control medium, mucin medium, CFS from *S. oris* grown in mucin medium, on normal human bronchial epithelia individually or in co-culture with *S. oris*. (B) Heatmap of amino acid transporter gene expression across conditions. (C) Expression of sialic acid catabolism (*nan* operon) genes. (D) Expression of glycogen metabolism genes (see Supplemental Files for complete gene lists). Each column in the heatmaps is an individual biological replicate, and each row is a transcript. Normalized read counts from DESeq2 are scaled by row and presented as Z-scores.

***F. nucleatum* amino acid uptake and metabolism**

Since *F. nucleatum* preferentially ferments amino acids, we surveyed the expression of genes involved in amino acid uptake (Fig. 2B) and metabolism (Fig. S3) to determine which substrates might be available across each growth medium or the airway epithelial environment. Two *brnQ* homologs encoding branched-chain amino acid (BCAA) importers and a *putP* proline transporter homolog were highly expressed in control medium, moderately expressed on NHBE, and showed the lowest expression in mucin medium, *S. oris* CFS (So CFS), and NHBE co-cultures. In contrast, homologs of the *azlC* and *azlD* BCAA importer family and a sodium:alanine symporter were upregulated in mucin medium and So CFS. Interestingly, the symporter exhibited low expression on NHBE alone but was elevated when *S. oris* was co-cultured on NHBE.

Several sodium-dependent symporters and transporters were specifically induced in So CFS, while multiple ABC-type transporters and permeases were selectively upregulated in NHBE co-culture, irrespective of *S. oris* presence. A sodium:proton antiporter and GntP-family permease were strongly induced in NHBE co-culture, but only in the presence of *S. oris*, suggesting interaction-dependent metabolic shifts. Genes involved in amino acid catabolism and short-chain fatty acid production were generally upregulated in NHBE co-culture with or without *S. oris*. Among these genes were those encoding butyrate production, which have recently been linked to reactive oxygen/nitrogen resistance in *F. nucleatum* (42). Overall, while these transcriptional patterns suggest condition-specific substrate utilization, further experimental validation will be required to define precise substrate specificities.

F. nucleatum* carbohydrate metabolism is modulated by *S. oris

Although *F. nucleatum* is known to catabolize glucose and fructose, other carbohydrate metabolic pathways were differentially expressed in So CFS and during co-culture with *S. oris* on NHBE cells. Because So CFS was derived from mucin medium-grown cultures, glycan degradation by *S. oris* could liberate component sugars that *F. nucleatum* subsequently metabolizes. For example, the *nan* operon (encoding a sialic acid catabolism pathway) was strongly induced in both So CFS and in NHBE co-culture conditions (Fig. 2C). Since *F. nucleatum* lacks a sialidase, its access to sialic acid is likely dependent on exogenous glycosidase activity from *S. oris*. The absence of *nan* induction in mucin medium supports this model.

F. nucleatum also encodes genes annotated for glycogen production and degradation though their function has not been experimentally confirmed. These genes were minimally expressed in control and mucin media but showed increased expression in So CFS and during NHBE co-culture, particularly when co-colonized with *S. oris* (Fig. 2D). This pattern suggests that glycogen-related pathways may participate in the utilization of glycan fragments generated by *S. oris*. Similarly, *F. nucleatum* encodes two putative α -1,4-polygalactosaminidases, enzymes that in some *Pseudomonas*, *Streptomyces*, and *Aspergillus* species degrade galactosaminoglycans such as chondroitin sulfate and dermatan sulfate (43–46). Although their expression was not strongly affected by the tested growth conditions, whether *F. nucleatum* homologs also degrade galactosaminoglycans remains to be determined. More broadly, numerous genes predicted to encode carbohydrate active enzymes (CAZymes) exhibited condition-dependent expression (Fig. S4). However, most of these are not involved in host glycan degradation, as they include functions related to cell wall homeostasis (*mrcB* homolog C7Y58_RS05695) and LPS assembly or modification (*lpxCB* genes).

Expression of *F. nucleatum* autotransporters and adhesins is modulated by nutrient and host conditions

Virulence in *F. nucleatum* is mediated by several Type V autotransporters that facilitate attachment to and invasion of host cells, and modulation of immune signaling (47–51). Therefore, we evaluated the expression of all annotated autotransporter genes across each broth and host-associated condition (Fig. S5). Expression clustered into three groups: (i) genes whose expression is highest in the control medium, (ii) those with elevated expression in mucin medium or So CFS (e.g., *radD*), and (iii) genes with maximal expression on NHBE in both mono- and co-culture. The latter group included several well-characterized *F. nucleatum* virulence factor genes, such as *fadA*, *cbpF*, fusolisins, and *fap2*. An interesting exception to this grouping was *fpIA*, which was highly expressed in control, mucin medium, and on NHBE, but was repressed in So CFS and in co-culture with *S. oris* on NHBE. These data are consistent with the increasing appreciation of the connections between bacterial metabolism and regulation of virulence factors and suggest that co-colonizing *S. oris* could modulate *fpIA*-mediated contributions to *F. nucleatum* virulence (52).

***S. oris* polysaccharide utilization loci expression is responsive to both host and *F. nucleatum* interactions**

The *S. oris* genome encodes 27 PULs and 1 putative CAZyme cluster, some homologous to validated systems in the *Bacteroides* genus (53, 54). Such systems are used by bacteria to sense and degrade polysaccharides typically found in plant fibers (e.g., xylan) or host glycans like mucins (55). We averaged the expression of each gene in every PUL to determine which PUL(s) respond to glycans present in mucin medium and on the apical surface of airway epithelial cells, as well as whether *F. nucleatum* supernatants or co-culture on epithelia modulate PUL expression (Fig. 3; File S3; Fig. S7). All but PUL9 were minimally expressed in control medium. Eleven PULs and the CAZyme cluster were induced in mucin medium, consistent with mucin glycan utilization. Unexpectedly, PUL

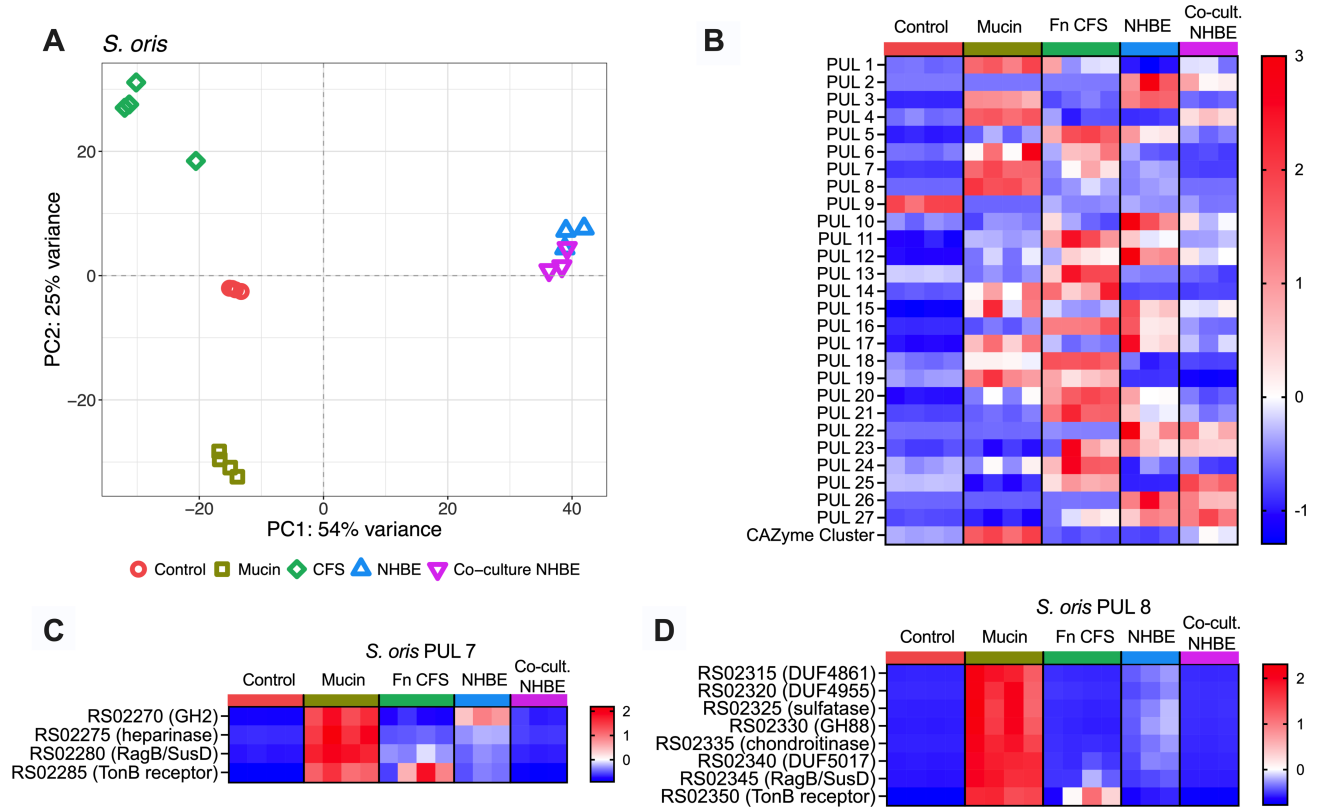


FIG 3 The *S. oris* transcriptome is significantly altered across media and co-culture conditions *in vitro*. (A) PCA of *S. oris* transcriptomes, colored by growth medium or co-culture status on NHBE, across growth conditions, lot depicting the transcriptome of individual *S. oris* samples, which are colored by growth medium or co-culture status on NHBE. Heatmaps of (B) average expression of every gene in a given PUL across conditions, (C) PUL 7, and (D) PUL 8 in *S. oris*. Data are scaled by row and presented as Z-scores. Statistical significance for PUL expression comparisons provided in File S4.

expression patterns were significantly altered in Fn CFS, with decreased expression of several mucin-induced PULs and induction of multiple mucin-insensitive PULs. A third group of PULs was induced during NHBE co-culture, including PULs 3, 5, 10, 12, and 15–17, many of which were suppressed in co-culture with *F. nucleatum*. In contrast, PULs 4 and 25, minimally expressed in NHBE monoculture, were induced by *F. nucleatum*. This variable expression of PULs was anticipated between growth in mucin medium and control media and on NHBE, but modulation of PUL expression in Fn CFS and co-culture on NHBE was unexpected. These data suggest that *F. nucleatum* may influence glycan foraging by *S. oris*, supporting a dynamic bidirectional interaction.

S. oris encodes a putative Type VI secretion system

Like many members of the Bacteroidota, *S. oris* encodes a predicted contact-dependent multi-protein Type VI secretion system (T6SS) that delivers toxins to adjacent bacteria in intensely competitive conditions (56). Given that *S. oris* typically resides in polymicrobial settings and, therefore, could plausibly benefit from such a system, we scanned the *S. oris* NCTC 13071 genome for T6SS genes using SecReT6 (File S4) (57). Three genomic loci were identified, including one containing 13 clear homologs of known T6SS genes and 2 smaller clusters each containing 4 homologs. Expression profiles (Fig. S8) revealed moderate expression in control medium and mucin media, with higher expression of select genes in Fn CFS. The *hcp* homolog was only expressed in control medium, while the *tssC* homolog was only expressed on NHBE, irrespective of the presence of *F. nucleatum*. A *tssI* homolog (locus tag EL210_RS03325) exhibited low-to-moderate expression across broth cultures and minimal expression in monoculture on NHBE but was highly induced in NHBE co-culture with *F. nucleatum*, suggesting potential functional

activation in response to interspecies contact. Given the lack of coordinated expression, it is unclear whether they comprise a functional T6SS and will require further experimental validation.

***F. nucleatum* drives airway epithelial inflammation, modulated by *S. oris* co-colonization**

We next profiled the transcriptional response of NHBE cells following 24 h colonization with *F. nucleatum* or *S. oris*, alone or in co-culture, relative to uninfected controls (Fig. 4A; Fig. S9, File S5). As expected, several mucin genes were expressed across all conditions, consistent with the presence of an epithelial mucus layer (Fig. S10). PCA analysis revealed that *S. oris* alone had little effect on the host transcriptome, whereas *F. nucleatum* induced a distinct and divergent host response. Co-colonization clustered separately from *F. nucleatum* monocolonization, suggesting *S. oris* modulates epithelial responses either directly or indirectly via interactions that modulate *F. nucleatum* virulence.

Gene set enrichment analysis (GSEA) (Fig. 4B; Files S6 and S7) identified enrichment of inflammation- and cancer-associated pathways in *F. nucleatum*-colonized epithelia, including TNF- α , IL-6/JAK/STAT3 signaling, IL-2/STAT5 signaling, and Wnt/ β -catenin signaling. Anti-inflammatory pathways were also suppressed, including downregulation of *HAS2*, which encodes hyaluronan synthase. Because hyaluronan is protective against airway inflammation and hyperresponsiveness, its suppression by *F. nucleatum* may exacerbate these processes in diseased airways (58).

Co-colonization with *S. oris* altered the NHBE transcriptome relative to monocolonization with either species, underscoring the influence of microbial interactions on host inflammatory signaling. For example, the most highly induced gene in co-colonized NHBEs relative to *F. nucleatum* alone was *PLEKHF2*, whose product is involved in micropinocytosis and TNF-driven apoptosis (59). *EDEM3*, associated with the unfolded protein response and endoplasmic reticulum stress (60), was also upregulated during co-colonization. Interestingly, *EDEM3* has been reported to translocate to the HeLa cell surface in response to the pore-forming listeriolysin O toxin from *Listeria monocytogenes* (61), suggesting possible parallels in epithelial stress responses.

Co-culture of both species on NHBE also influenced the expression of genes that were uniquely enriched relative to *F. nucleatum* mono-colonization (Fig. 4C and D). Some inflammatory markers, such as *IL1- β* , were induced by *F. nucleatum* alone and did not change in co-culture, while others, including *SQLE* (encoding squalene epoxidase), were upregulated only under co-colonization conditions. Together, these data reveal that (i) *F. nucleatum* elicits a strong pro-inflammatory transcriptional program in airway epithelial cells and (ii) co-colonization with *S. oris* further reshapes this response, highlighting complex, interspecies interactions that modulate host inflammation in ways not apparent during monocolonization.

DISCUSSION

The frequent co-colonization of *F. nucleatum* and *S. oris* across mucosal environments suggests potential functional interactions that influence bacterial colonization, persistence, and host responses. Using both *in vitro* and airway epithelial culture models, we show that these species engage in bidirectional interactions involving glycan degradation, metabolite exchange, and transcriptional modulation. Although some transcriptional overlaps were observed, the global gene expression profiles of both species in broth culture differed markedly from those during epithelial colonization, particularly in pathways related to metabolism and *F. nucleatum* virulence regulation. These differences likely reflect two non-mutually exclusive factors: (i) the distinct physical and nutritional environments of liquid culture vs the static, host-associated surface of NHBEs and/or (ii) variation in bacterial growth phase between conditions. Although CFUs were not measured for either species on NHBEs to directly assess growth phase, these findings underscore the importance of modeling microbial interactions under physiologically relevant conditions. Transcriptomic analyses were performed on 24 h cultures

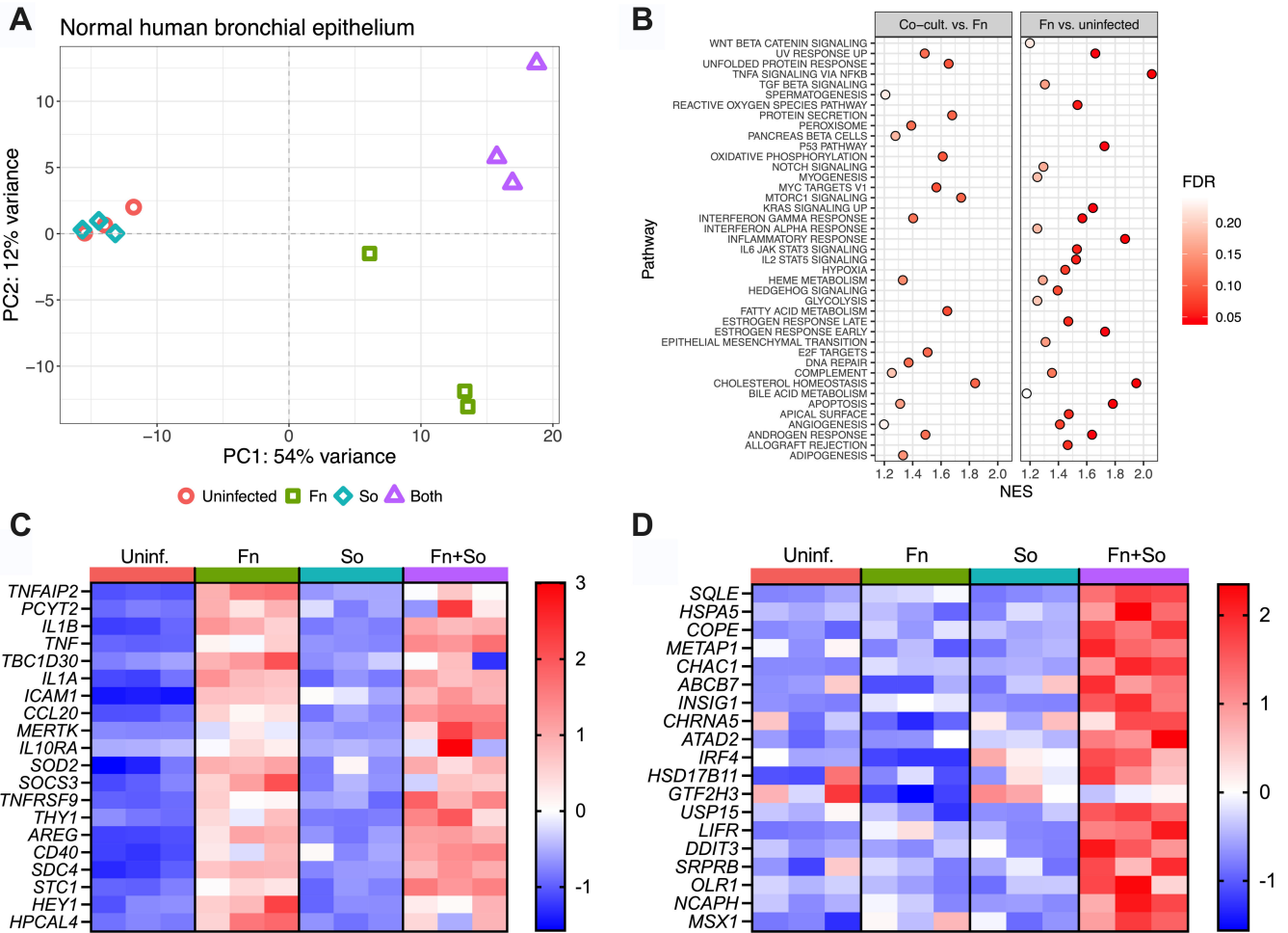


FIG 4 Bacterial colonization alters the NHBE transcriptome. (A) PCA plot of host transcriptomes following mono- and co-colonization with *F. nucleatum* and *S. oris*. (B) Gene set enrichment analysis (GSEA) in samples from NHBE colonized with both *F. nucleatum* and *S. oris* compared to mono-colonization with *F. nucleatum* (left) and NHBE mono-colonized with *F. nucleatum* compared to uninfected cells. Normalized enrichment scores (NES) are shown on the x-axis, and the color of each point indicates false discovery rate (FDR). High NES with low FDR indicates a pathway enriched in a given comparison. Pathways enriched in both comparisons were removed from the Co-cult versus Fn plot to highlight pathways unique to this comparison, and only those pathways with an FDR < 0.25 are shown. Expression heatmaps of transcripts enriched in (C) cells mono-colonized with *F. nucleatum* or (D) cells dual-colonized with *F. nucleatum* and *S. oris*. Data in panels C and D are scaled by row and presented as Z-scores.

corresponding to early stationary phase for both species (Fig. 1A and D), a time point that captured active metabolism while minimizing nutrient depletion. Nonetheless, inherent growth differences between *F. nucleatum* and *S. oris* may also contribute to the observed variability in gene expression.

Despite these contextual differences, two transcriptional signals indicative of glycan-mediated interactions were consistently observed across both culture and host-associated conditions. First, the *F. nucleatum nan* operon, which encodes a sialic acid catabolism pathway, was not expressed in mucin medium but was strongly induced in *S. oris* supernatants and during co-colonization on NHBE cells. Given that *F. nucleatum* lacks sialidase activity, these data support a model in which sialic acid utilization depends on glycosidase activity from co-resident microbiota. This finding is consistent with previous work (28) that showed that *F. nucleatum* exploits sialidase-positive species to access host-derived sialic acids in dysbiotic vaginal communities. Although the *nan* operon is not conserved across all *F. nucleatum* subspecies, the broader concept of *F. nucleatum* promoting dysbiotic bacterial community structures through metabolic cross-feeding likely extends to multiple mucosal environments. Indeed, Queen et al. identified *F.*

nucleatum within polymicrobial biofilms on colorectal tumors and noted enrichment of sialic acid-adjacent metabolic pathways (62). Similarly, *F. nucleatum* was shown to bind to and interact with *Clostridioides difficile* on MUC2-coated surfaces in a bioreactor model, promoting biofilm formation and broad transcriptional changes in *C. difficile*, including metabolic reprogramming (63). Furtado et al. further observed induction of a fructose/mannose PTS system when *C. difficile* was grown in the mucus layer of intestinal epithelial cells *in vitro* (64). Interestingly, we also detected increased expression of a homologous system in *F. nucleatum* grown in mucin. Although our study focused on transcriptional responses, future biochemical analyses of cell-free supernatants (e.g., LC-MS) will be important to identify specific metabolites exchanged between species and to validate the cross-feeding interactions inferred here.

A second glycan-associated transcriptional signal involved modulation of *S. oris* PULs. While several PULs were robustly induced by mucin medium, their expression was suppressed in the presence of *F. nucleatum* supernatants or during co-colonization on epithelial cells. This is notable for two reasons: (i) the large number of PULs affected and (ii) the fact that *F. nucleatum* has not been reported to degrade host-associated glycans and is, therefore, not expected to appreciably alter the glycan landscape of mucin medium. Porcine gastric mucin used in this study is a crude proteolytic digest and likely contains non-mucin glycans such as glycosaminoglycans, which may explain the broad induction of PULs. For example, PULs predicted to target heparin and chondroitin (e.g., PULs 7 and 8) were induced in both mucin medium and on NHBE cells but were repressed in the presence of *F. nucleatum*, suggesting nutrient depletion or transcriptional repression. One possible mechanism is that *F. nucleatum* secretes metabolic byproducts that modulate *S. oris* gene expression. These products could include secreted polyglucose or glycogen, which could then be available to *S. oris* or scavenged from dead *F. nucleatum* cells. Notably, *F. nucleatum* glycogen metabolism genes were upregulated on NHBE, particularly during co-culture with *S. oris*, but not in mucin medium, suggesting that glycogen is unlikely to be present in *Fusobacterium* supernatants.

The airway epithelial response was strongly influenced by *F. nucleatum* and further modulated by co-colonization with *S. oris*. Consistent with prior single-cell RNA-seq studies (41), *F. nucleatum* elicited robust inflammatory signaling, including induction of *TNF- α* , *IL-1 β* , and mitochondrial stress responses suggestive of apoptosis. In contrast, NHBE colonized with *S. oris* alone exhibited no differentially expressed genes compared to controls, consistent with its commensal nature. Nevertheless, co-colonization with *S. oris* altered the epithelial response, indicating that microbial interactions can modulate host sensing and inflammation. For example, *TNS4*, a gene linked to poor prognosis in lung adenocarcinoma (65), was significantly downregulated in NHBEs co-colonized with *S. oris* and *F. nucleatum* relative to *F. nucleatum* alone. Conversely, co-culture induced expression of several genes not responsive to either bacterium individually (Fig. 4D). Because *S. oris* alone had minimal effect, we hypothesize that co-colonization alters *F. nucleatum* behavior in ways that modulate host responses. However, we cannot rule out *F. nucleatum*-driven changes in *S. oris* behavior that directly influence the airway epithelial response. Regardless, these data collectively highlight the need to consider microbial interactions when modeling host-pathogen dynamics and support integrating microbiome-derived hypotheses with mechanistic approaches to uncover host-pathogen-microbiome interactions.

In summary, our findings demonstrate that interactions between nutrient availability, the host environment, and co-colonizing bacteria shape the behavior of *F. nucleatum*, *S. oris*, and airway epithelial cells. Limitations should be acknowledged. While transcriptional and translational outputs are generally correlated, differences in mRNA and protein stability may result in temporal or spatial discrepancies in bacterial and host behavior that are not captured here. Likewise, site-directed mutagenesis is required to confirm several bacterial interactions suggested by our data, but genetic tools for *F. nucleatum* are only recently emerging and remain unavailable for *S. oris*. Finally, we evaluated only one strain of each species, which constrains our ability to assess strain-

and subspecies-level genetic (and thus phenotypic) diversity. Despite these limitations, our results provide a framework for exploring glycan-driven cross-feeding and its impact on pathobiont behavior and host responses in mucosal environments.

ACKNOWLEDGMENTS

This work was funded by the National Institute for Allergy and Infectious Diseases (AI177613), the University at Buffalo Research Foundation, and a Cystic Fibrosis Foundation postdoctoral fellowship to J.R.F. (002569F221).

AUTHOR AFFILIATIONS

¹Department of Population Health and Pathobiology, North Carolina State University College of Veterinary Medicine, Raleigh, North Carolina, USA

²Department of Microbiology & Immunology, Jacobs School of Medicine and Biomedical Sciences, University at Buffalo, Buffalo, New York, USA

AUTHOR ORCIDs

Joshua R. Fletcher  <http://orcid.org/0000-0002-0723-3195>

Ryan C. Hunter  <http://orcid.org/0000-0003-3841-1676>

FUNDING

Funder	Grant(s)	Author(s)
National Institute of Allergy and Infectious Diseases	AI177613	Ryan C. Hunter
Cystic Fibrosis Foundation	002569F221	Joshua R. Fletcher

AUTHOR CONTRIBUTIONS

Joshua R. Fletcher, Conceptualization, Data curation, Formal analysis, Funding acquisition, Investigation, Methodology, Project administration, Visualization, Writing – original draft, Writing – review and editing | Areej Malik, Investigation | Jacob Driggers, Investigation | Ryan C. Hunter, Conceptualization, Data curation, Funding acquisition, Resources, Supervision, Visualization, Writing – original draft, Writing – review and editing

DATA AVAILABILITY

All sequencing files are available at the NCBI Sequence Read Archive (SRA) under accession number [PRJNA1282640](#).

ADDITIONAL FILES

The following material is available [online](#).

Supplemental Material

File S1 (mSystems00922-25-s0001.xlsx). All differentially expressed genes in *F. nucleatum* across the growth conditions in this study.

File S2 (mSystems00922-25-s0002.xlsx). All differentially expressed genes in *S. oris* across the growth conditions in this study.

File S3 (mSystems00922-25-s0003.xlsx). ANOVA results comparing averaged PUL in *S. oris* across all growth conditions in this study.

File S4 (mSystems00922-25-s0004.xlsx). *S. oris* genes predicted by SecReT6 to be homologs of type 6 secretion system genes.

File S5 (mSystems00922-25-s0005.xlsx). GSEA of NHBE incubated with *F. nucleatum* for 24 hours compared to uninfected NHBE.

File S6 (mSystems00922-25-s0006.xlsx). GSEA of NHBE incubated with *F. nucleatum* for 24 hours compared to uninfected NHBE.

File S7 (mSystems00922-25-s0007.xlsx). GSEA of NHBE incubated with *F. nucleatum* and *S. oris* for 24 hours compared to NHBE incubated with *F. nucleatum* alone.
Supplemental Figures (mSystems00922-25-s0008.pdf). Figures S1 to S10.

REFERENCES

- Segata N, Haake SK, Mannon P, Lemon KP, Waldron L, Gevers D, Huttenhower C, Izard J. 2012. Composition of the adult digestive tract bacterial microbiome based on seven mouth surfaces, tonsils, throat and stool samples. *Genome Biol* 13:R42. <https://doi.org/10.1186/gb-2012-13-6-r42>
- Loozen G, Ozelik O, Boon N, De Mol A, Schoen C, Quirynen M, Teughels W. 2014. Inter-bacterial correlations in subgingival biofilms: a large-scale survey. *J Clin Periodontol* 41:1–10. <https://doi.org/10.1111/jcpe.12167>
- Kostic AD, Gevers D, Pedamallu CS, Michaud M, Duke F, Earl AM, Ojesina AI, Jung J, Bass AJ, Tabernero J, Baselga J, Liu C, Shivdasani RA, Ogino S, Birren BW, Huttenhower C, Garrett WS, Meyerson M. 2012. Genomic analysis identifies association of *Fusobacterium* with colorectal carcinoma. *Genome Res* 22:292–298. <https://doi.org/10.1101/gr.126573.111>
- Tahara S, Shijimaya T, Yamazaki J, Kobayashi S, Horitani A, Matsumoto Y, Nakamura N, Okazaki T, Takahashi Y, Tomiyama T, Honzawa Y, Fukata N, Fukui T, Naganuma M. 2024. *Fusobacterium* detected in barrett's esophagus and esophageal adenocarcinoma tissues. *Cancer Invest* 42:469–477. <https://doi.org/10.1080/07357907.2024.2359980>
- Battaglia TW, Mimpfen IL, Traets JH, van Hoeck A, Zevenrijn LJ, Geurts BS, de Wit GF, Noë M, Hofland I, Vos JL, Cornelissen S, Alkemade M, Broeks A, Zuur CL, Cuppen E, Wessels L, van de Haar J, Voest E. 2024. A pan-cancer analysis of the microbiome in metastatic cancer. *Cell* 187:2324–2335. <https://doi.org/10.1016/j.cell.2024.03.021>
- Zhang JW, Zhang D, Yin HS, Zhang H, Hong KQ, Yuan JP, Yu BP. 2023. *Fusobacterium nucleatum* promotes esophageal squamous cell carcinoma progression and chemoresistance by enhancing the secretion of chemotherapy-induced senescence-associated secretory phenotype via activation of DNA damage response pathway. *Gut Microbes* 15:2197836. <https://doi.org/10.1080/19490976.2023.2197836>
- Lucas SK, Yang R, Dunitz JM, Boyer HC, Hunter RC. 2018. 16S rRNA gene sequencing reveals site-specific signatures of the upper and lower airways of cystic fibrosis patients. *J Cyst Fibros* 17:204–212. <https://doi.org/10.1016/j.jcf.2017.08.007>
- Lucas SK, Feddema E, Boyer HC, Hunter RC. 2021. Diversity of cystic fibrosis chronic rhinosinusitis microbiota correlates with different pathogen dominance. *J Cyst Fibros* 20:678–681. <https://doi.org/10.1016/j.jcf.2021.03.022>
- Lucas SK, Villarreal AR, Ahmad MM, Itabiyi A, Feddema E, Boyer HC, Hunter RC. 2021. Anaerobic microbiota derived from the upper airways impact *Staphylococcus aureus* physiology. *Infect Immun* 89:e00153-21. <https://doi.org/10.1128/IAI.00153-21>
- Thornton CS, Surette MG. 2021. Potential contributions of anaerobes in cystic fibrosis airways. *J Clin Microbiol* 59:e01813-19. <https://doi.org/10.1128/JCM.01813-19>
- Pappe E, Hübner R-H, Saccomanno J, Ebrahimi HDN, Witzernath M, Wiessner A, Sarbandi K, Xiong Z, Kursawe L, Moter A, Kikhney J. 2024. Biofilm infections of endobronchial valves in COPD patients after endoscopic lung volume reduction: a pilot study with FISHseq. *Sci Rep* 14:23078. <https://doi.org/10.1038/s41598-024-73950-3>
- Choi YJ, Park HJ, Kim CY, Choi A, Cho JH, Byun MK. 2025. Dynamic microbial changes in exacerbation of chronic obstructive pulmonary disease. *Front Microbiol* 15:1507090. <https://doi.org/10.3389/fmicb.2024.1507090>
- Bahetjan K, Lin S, Aili N, Yang H, Du S. 2025. Analysis of the bronchoalveolar lavage fluid microbial flora in COPD patients at different lung function during acute exacerbation. *Sci Rep* 15:13179. <https://doi.org/10.1038/s41598-025-96746-5>
- O'Farrell HE, Shaw JG, Goh F, Bowman RV, Fong KM, Krause L, Yang IA. 2019. Potential clinical utility of multiple target quantitative polymerase chain reaction (qPCR) array to detect microbial pathogens in patients with chronic obstructive pulmonary disease (COPD). *J Thorac Dis* 11:S2254–S2265. <https://doi.org/10.21037/jtd.2019.10.39>
- Hendrickson EL, Wang T, Beck DAC, Dickinson BC, Wright CJ, Lamont R, Hackett M. 2014. Proteomics of *Fusobacterium nucleatum* within a model developing oral microbial community. *Microbiol Open* 3:729–751. <https://doi.org/10.1002/mbo3.204>
- Zelasko S, Swaney MH, Sandstrom S, Lee KE, Dixon J, Riley C, Watson L, Godfrey JJ, Ledrowski N, Rey F, Safdar N, Seroogy CM, Gern JE, Kalan L, Currie C. 2025. Early-life upper airway microbiota are associated with decreased lower respiratory tract infections. *J Allergy Clin Immunol* 155:436–450. <https://doi.org/10.1016/j.jaci.2024.11.008>
- Sato T, Kamaguchi A, Nakazawa F. 2012. The release of glyceraldehyde-3-phosphate dehydrogenase (GAPDH) from human erythrocyte membranes lysed by hemolysin of *Prevotella oris*. *Anaerobe* 18:553–555. <https://doi.org/10.1016/j.anaerobe.2012.08.008>
- Hong B-Y, Sobue T, Choquette L, Dupuy AK, Thompson A, Burleson JA, Salner AL, Schauer PK, Joshi P, Fox E, Shin D-G, Weinstock GM, Strausbaugh LD, Dongari-Bagtzoglou A, Peterson DE, Diaz PI. 2019. Chemotherapy-induced oral mucositis is associated with detrimental bacterial dysbiosis. *Microbiome* 7:66. <https://doi.org/10.1186/s40168-019-0679-5>
- Dicksved J, Lindberg M, Rosenquist M, Enroth H, Jansson JK, Engstrand L. 2009. Molecular characterization of the stomach microbiota in patients with gastric cancer and in controls. *J Med Microbiol* 58:509–516. <https://doi.org/10.1099/jmm.0.007302-0>
- Greathouse KL, Stone JK, Vargas AJ, Choudhury A, Padgett RN, White JR, Jung A, Harris CC. 2024. Co-enrichment of cancer-associated bacterial taxa is correlated with immune cell infiltrates in esophageal tumor tissue. *Sci Rep* 14:2574. <https://doi.org/10.1038/s41598-023-48862-3>
- McCoy AN, Araújo-Pérez F, Azcárate-Peril A, Yeh JJ, Sandler RS, Keku TO. 2013. *Fusobacterium* is associated with colorectal adenomas. *PLoS One* 8:e53653. <https://doi.org/10.1371/journal.pone.0053653>
- Dzink JL, Socransky SS. 1990. Amino acid utilization by *Fusobacterium nucleatum* grown in a chemically defined medium. *Oral Microbiol Immunol* 5:172–174. <https://doi.org/10.1111/j.1399-302x.1990.tb00418.x>
- Zilm PS, Gully NJ, Rogers AH. 2002. Growth pH and transient increases in amino acid availability influence polyglucose synthesis by *Fusobacterium nucleatum* grown in continuous culture. *FEMS Microbiol Lett* 215:203–208. <https://doi.org/10.1111/j.1574-6968.2002.tb11392.x>
- Rogers AH, Chen J, Zilm PS, Gully NJ. 1998. The behaviour of *Fusobacterium nucleatum* chemostat-grown in glucose- and amino acid-based chemically defined media. *Anaerobe* 4:111–116. <https://doi.org/10.1006/anae.1997.0140>
- Zilm PS, Gully NJ, Rogers AH. 2003. Changes in growth and polyglucose synthesis in response to fructose metabolism by *Fusobacterium nucleatum* grown in continuous culture. *Oral Microbiol Immunol* 18:260–262. <https://doi.org/10.1034/j.1399-302x.2003.00069.x>
- Rogers AH, Zilm PS, Gully NJ, Pfennig AL, Marsh PD. 1991. Aspects of the growth and metabolism of *Fusobacterium nucleatum* ATCC 10953 in continuous culture. *Oral Microbiol Immunol* 6:250–255. <https://doi.org/10.1111/j.1399-302x.1991.tb00486.x>
- Rogers AH, Zilm PS. 1995. The influence of intracellular polyglucose and prior growth rate on the survival of *Fusobacterium nucleatum* under starvation conditions. *Oral Microbiol Immunol* 10:119–121. <https://doi.org/10.1111/j.1399-302x.1995.tb00130.x>
- Agarwal K, Robinson LS, Aggarwal S, Foster LR, Hernandez-Leyva A, Lin H, Tortelli BA, O'Brien VP, Miller L, Kau AL, Reno H, Gilbert NM, Lewis WG, Lewis AL. 2020. Glycan cross-feeding supports mutualism between *Fusobacterium* and the vaginal microbiota. *PLoS Biol* 18:e3000788. <https://doi.org/10.1371/journal.pbio.3000788>
- Terrapon N, Lombard V, Gilbert HJ, Henrissat B. 2015. Automatic prediction of polysaccharide utilization loci in bacteroidetes species. *Bioinformatics* 31:647–655. <https://doi.org/10.1093/bioinformatics/btu716>
- Terrapon Nicolas, Lombard V, Drula É, Lapébie P, Al-Masaudi S, Gilbert HJ, Henrissat B. 2018. PULDB: the expanded database of polysaccharide utilization loci. *Nucleic Acids Res* 46:D677–D683. <https://doi.org/10.1093/nar/gkx1022>
- Marsili E, Rollefson JB, Baron DB, Hozalski RM, Bond DR. 2008. Microbial biofilm voltammetry: direct electrochemical characterization of catalytic electrode-attached biofilms. *Appl Environ Microbiol* 74:7329–7337. <https://doi.org/10.1128/AEM.00177-08>

32. Flynn JM, Niccum D, Dunitz JM, Hunter RC. 2016. Evidence and role for bacterial mucin degradation in cystic fibrosis airway disease. *PLoS Pathog* 12:e1005846. <https://doi.org/10.1371/journal.ppat.1005846>
33. Merritt JH, Kadouri DE, O'Toole GA. 2005. Growing and analyzing static biofilms. *Curr Protoc Microbiol* 00:1B.1.1–1B.1.17. <https://doi.org/10.1002/9780471729259.mc01b01s00>
34. Rayner RE, Makena P, Prasad GL, Cormet-Boyaka E. 2019. Optimization of normal human bronchial epithelial (NHBE) cell 3D cultures for *in vitro* lung model studies. *Sci Rep* 9:500. <https://doi.org/10.1038/s41598-018-36735-z>
35. Munye MM, Shoemark A, Hirst RA, Delhove JM, Sharp TV, McKay TR, O'Callaghan C, Baines DL, Howe SJ, Hart SL. 2017. BMI-1 extends proliferative potential of human bronchial epithelial cells while retaining their mucociliary differentiation capacity. *Am J Physiol Lung Cell Mol Physiol* 312:L258–L267. <https://doi.org/10.1152/ajplung.00471.2016>
36. Williams CR, Baccarella A, Parrish JZ, Kim CC. 2016. Trimming of sequence reads alters RNA-Seq gene expression estimates. *BMC Bioinform* 17:103. <https://doi.org/10.1186/s12859-016-0956-2>
37. Patro R, Duggal G, Love MI, Irizarry RA, Kingsford C. 2017. Salmon provides fast and bias-aware quantification of transcript expression. *Nat Methods* 14:417–419. <https://doi.org/10.1038/nmeth.4197>
38. Soneson C, Love MI, Robinson MD. 2015. Differential analyses for RNA-seq: transcript-level estimates improve gene-level inferences. *F1000Res* 4:1521. <https://doi.org/10.12688/f1000research.7563.2>
39. Love MI, Huber W, Anders S. 2014. Moderated estimation of fold change and dispersion for RNA-seq data with DESeq2. *Genome Biol* 15:550. <https://doi.org/10.1186/s13059-014-0550-8>
40. Kaplan CW, Lux R, Haake SK, Shi W. 2009. The *Fusobacterium nucleatum* outer membrane protein RadD is an arginine-inhibitable adhesin required for inter-species adherence and the structured architecture of multispecies biofilm. *Mol Microbiol* 71:35–47. <https://doi.org/10.1111/j.1365-2958.2008.06503.x>
41. Moore PJ, Hoffman K, Ahmed S, Fletcher JR, Wiggen TD, Lucas SK, Arif SJ, Gilbertsen AJ, Kent LA, Fiege JK, Langlois RA, O'Grady SM, Hunter RC. 2025. Dual oxic-anoxic co-culture enables direct study of anaerobe–host interactions at the airway epithelial interface. *mBio* 16:e01338-24. <https://doi.org/10.1128/mbio.01338-24>
42. Bystrom LT, Wolthers KR. 2024. New electron-transfer chain to a flavodiiron protein in *Fusobacterium nucleatum* couples butyryl-CoA oxidation to O₂ reduction. *Biochemistry* 63:2352–2368. <https://doi.org/10.1021/acs.biochem.4c00279>
43. Bamford NC, Le Mauff F, Subramanian AS, Yip P, Millán C, Zhang Y, Zacharias C, Forman A, Nitz M, Codée JDC, Usón I, Sheppard DC, Howell PL. 2019. Ega3 from the fungal pathogen *Aspergillus fumigatus* is an endo- α -1,4-galactosaminidase that disrupts microbial biofilms. *J Biol Chem* 294:13833–13849. <https://doi.org/10.1074/jbc.RA119.009910>
44. Reissig JL, Lai WH, Glasgow JE. 1975. An endogalactosaminidase from *Streptomyces griseus*. *Can J Biochem* 53:1237–1249. <https://doi.org/10.1139/o75-169>
45. Tamura J, Abe T, Hasegawa K, Kadowaki K. 1992. The mode of action of endo α -1,4 polygalactosaminidase from *Pseudomonas* sp. 881 on galactosaminooligosaccharides. *Biosci Biotechnol Biochem* 56:380–383. <https://doi.org/10.1271/bbb.56.380>
46. Pomin VH, Vignovich WP, Gonzales AV, Vasconcelos AA, Mulloy B. 2019. Galactosaminoglycans: medical applications and drawbacks. *Molecules* 24:2803. <https://doi.org/10.3390/molecules24152803>
47. Casasanta MA, Yoo CC, Smith HB, Duncan AJ, Cochran K, Varano AC, Allen-Vercoe E, Slade DJ. 2017. A chemical and biological toolbox for type Vd secretion: characterization of the phospholipase A1 autotransporter FplA from *Fusobacterium nucleatum* *J Biol Chem* 292:20240–20254. <https://doi.org/10.1074/jbc.M117.819144>
48. Doron L, Copenhagen-Glazer S, Ibrahim Y, Eini A, Naor R, Rosen G, Bachrach G. 2014. Identification and characterization of fusolisins, the *Fusobacterium nucleatum* autotransporter serine protease. *PLoS One* 9:e111329. <https://doi.org/10.1371/journal.pone.0111329>
49. Gur C, Ibrahim Y, Isaacson B, Yamin R, Abed J, Gamliel M, Enk J, Bar-On Y, Stanietsky-Kaynan N, Copenhagen-Glazer S, Shussman N, Almog G, Cuapio A, Hofer E, Mevorach D, Tabib A, Ortenberg R, Markel G, Miklič K, Jonjic S, Brennan CA, Garrett WS, Bachrach G, Mandelboim O. 2015. Binding of the Fap2 protein of *Fusobacterium nucleatum* to human inhibitory receptor TIGIT protects tumors from immune cell attack. *Immunity* 42:344–355. <https://doi.org/10.1016/j.immuni.2015.01.010>
50. Abed J, Emgård JEM, Zamir G, Faroja M, Almog G, Grenov A, Sol A, Naor R, Pikarsky E, Atlan KA, Mellul A, Chaushu S, Manson AL, Earl AM, Ou N, Brennan CA, Garrett WS, Bachrach G. 2016. Fap2 mediates *Fusobacterium nucleatum* colorectal adenocarcinoma enrichment by binding to tumor-expressed Gal-GalNAc. *Cell Host Microbe* 20:215–225. <https://doi.org/10.1016/j.chom.2016.07.006>
51. Meng Q, Gao Q, Mehrzarin S, Tangwanichapong K, Wang Y, Huang Y, Pan Y, Robinson S, Liu Z, Zangiabadi A, Lux R, Papapanou PN, Guo XE, Wang H, Berchowitz LE, Han YW. 2021. *Fusobacterium nucleatum* secretes amyloid-like FadA to enhance pathogenicity. *EMBO Rep* 22:e52891. <https://doi.org/10.15252/embr.202152891>
52. Rohmer L, Hocquet D, Miller SI. 2011. Are pathogenic bacteria just looking for food? metabolism and microbial pathogenesis. *Trends Microbiol* 19:341–348. <https://doi.org/10.1016/j.tim.2011.04.003>
53. Drula E, Garron M-L, Dogan S, Lombard V, Henrissat B, Terrapon N. 2022. The carbohydrate-active enzyme database: functions and literature. *Nucleic Acids Res* 50:D571–D577. <https://doi.org/10.1093/nar/gkab1045>
54. Zheng J, Ge Q, Yan Y, Zhang X, Huang L, Yin Y. 2023. dbCAN3: automated carbohydrate-active enzyme and substrate annotation. *Nucleic Acids Res* 51:W115–W121. <https://doi.org/10.1093/nar/gkad328>
55. Glowacki RWP, Martens EC. 2020. If you eat it, or secrete it, they will grow: the expanding list of nutrients utilized by human gut bacteria. *J Bacteriol* 203:e00481-20. <https://doi.org/10.1128/JB.00481-20>
56. Coyne MJ, Comstock LE. 2019. Type VI secretion systems and the gut microbiota. *Microbiol Spectr* 7:psib-0009-2018. <https://doi.org/10.1128/microbiolspec.psib-0009-2018>
57. Zhang J, Guan J, Wang M, Li G, Djordjevic M, Tai C, Wang H, Deng Z, Chen Z, Ou HY. 2023. SecReT6 update: a comprehensive resource of bacterial type VI secretion systems. *Sci China Life Sci* 66:626–634. <https://doi.org/10.1007/s11427-022-2172-x>
58. Tsunoda Y, Sherpa MT, Kiwamoto T, Matsuyama M, Osawa H, Sakurai H, Hayashi S, Matsuno Y, Morishima Y, Ishii Y, Hizawa N. 2021. Has2 deficiency enhances OVA-induced airway inflammation and hyperresponsiveness in mice. *Allergy* 76:2214–2218. <https://doi.org/10.1111/all.14715>
59. Li C, Liu Q, Li N, Chen W, Wang L, Wang Y, Yu Y, Cao X. 2008. EAPF/Phafin-2, a novel endoplasmic reticulum-associated protein, facilitates TNF-alpha-triggered cellular apoptosis through endoplasmic reticulum-mitochondrial apoptotic pathway. *J Mol Med (Berlin)* 86:471–484. <https://doi.org/10.1007/s00109-007-0298-7>
60. Moretti J, Roy S, Bozec D, Martinez J, Chapman JR, Ueberheide B, Lamming DW, Chen ZJ, Horng T, Yeretssian G, Green DR, Blander JM. 2017. STING senses microbial viability to orchestrate stress-mediated autophagy of the endoplasmic reticulum. *Cell* 171:809–823. <https://doi.org/10.1016/j.cell.2017.09.034>
61. Kühbacher A, Novy K, Quereda JJ, Sachse M, Moya-Nilges M, Wollscheid B, Cossart P, Pizarro-Cerdá J. 2018. Listeriolysin O-dependent host surfaceome remodeling modulates *Listeria monocytogenes* invasion. *Pathog Dis* 76:ft082. <https://doi.org/10.1093/femspd/ft082>
62. Queen J, Cing Z, Minsky H, Nandi A, Southward T, Ferri J, McManm M, Iyadorai T, Vadivelu J, Roslani A, Loke MF, Wanyiri J, White JR, Drewes JL, Sears CL. 2025. *Fusobacterium nucleatum* is enriched in invasive biofilms in colorectal cancer. *NPJ Biofilms Microbiomes* 11:81. <https://doi.org/10.1038/s41522-025-00717-7>
63. Engevik MA, Danhof HA, Auchtung J, Endres BT, Ruan W, Bassères E, Engevik AC, Wu Q, Nicholson M, Luna RA, Garey KW, Crawford SE, Estes MK, Lux R, Yacyshyn MB, Yacyshyn B, Savidge T, Britton RA, Versalovic J. 2021. *Fusobacterium nucleatum* adheres to *Clostridioides difficile* via the RadD adhesin to enhance biofilm formation in intestinal mucus. *Gastroenterology* 160:1301–1314. <https://doi.org/10.1053/j.gastro.2020.11.034>
64. Furtado KL, Plott L, Markovetz M, Powers D, Wang H, Hill DB, Papin J, Allbritton NL, Tamayo R. 2024. *Clostridioides difficile*-mucus interactions encompass shifts in gene expression, metabolism, and biofilm formation. *mSphere* 9:e00081-24. <https://doi.org/10.1128/msphere.00081-24>
65. Liu F, Gao X, Liu W, Xue W. 2022. Mining TCGA and GEO databases for the prediction of poor prognosis in lung adenocarcinoma based on up-regulated expression of TNS4. *Medicine (Baltimore)* 101:e31120. <https://doi.org/10.1097/MD.00000000000031120>